The effect of organic matter type on formation and evolution of diamondoids

3 authors:

Jiang Wenmin
Chinese Academy of Sciences
7 PUBLICATIONS **20** CITATIONS

SEE PROFILE

Yun Li
Guangzhou Institute of Geochemistry, Chinese Academy of Science
25 PUBLICATIONS **252** CITATIONS

SEE PROFILE

Yongqiang Xiong
Chinese Academy of Sciences
81 PUBLICATIONS **696** CITATIONS

SEE PROFILE

Some of the authors of this publication are also working on these related projects:

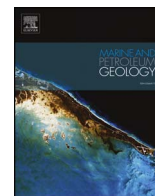Project The formation and evolution of solid bitumens originating from thermal cracking View project

Project Characterizing nanomechanical properties of shales via AFM and Nanoindentation View project

Research paper

The effect of organic matter type on formation and evolution of diamondoids

Wenmin Jiang[a,b], Yun Li[a,*], Yongqiang Xiong[a]

[a] State Key Laboratory of Organic Geochemistry (SKLOG), Guangzhou Institute of Geochemistry, Chinese Academy of Sciences, Guangzhou 510640, PR China
[b] University of Chinese Academy of Sciences, Beijing 10039, PR China

ARTICLE INFO

ABSTRACT

A series of anhydrous pyrolysis experiments, using sealed gold tubes, were performed on three types of kerogen to investigate the effect organic matter type has on the generation and evolution of thermogenic diamondoids. Based on the compositional variation of pyrolysis products, the cracking of kerogens can be divided into three stages: oil generation (0.6%–1.5% EasyRo), wet-gas generation (1.5%–2.1% EasyRo) and dry-gas generation (> 2.1% EasyRo). The experimental results indicate that diamondoids were mainly generated in the oil and wet-gas generation stages and decomposed in the dry-gas generation stage. In addition to thermal maturity, the formation of diamondoids is also influenced by the type of organic matter. Type I and II_A kerogens produced more diamondoids than Type III kerogen, and diamondoids generated from Type III kerogen were dominantly adamantanes. Therefore, the concentration and concentration ratios of diamondoids can be used to assess the maturity of source rocks (1.0%–1.5% EasyRo) and determine the type of organic matter (1.0%–2.0% EasyRo). Isomerization ratios of diamondoids depend mainly on thermal maturity and the type of organic matter has little effect. The use of isomerization ratios to determine thermal maturity is best for source rocks at higher maturity levels (1.5%–3.0% EasyRo). Therefore, bivariate diagrams of concentration versus isomerization indices of diamondoids (e.g., DMAs/MDs vs. DMAI-1 and DMAs/MDs vs. TMAI-1) can be used to evaluate the source rock maturity over a wider EasyRo range (1.0%–3.0% EasyRo) than single diamondoid parameters. As there are differences in the concentration and distribution of diamondoids in the extracts of three source rocks, the possibility exists to use diamondoid indices of immature rocks to determine the type of source rock.

1. Introduction

Diamondoids are rigid fused-ring alkanes with diamond-like structures. After adamantane was first recognized in crude oil from Czechoslovakia in 1933 (Landa and Machacek, 1933), diamondoids have been identified in crude oil from different basins (Williams et al., 1986; Wingert, 1992; Chen et al., 1996; Dahl et al., 1999), coal deposits, and sedimentary rocks (Schulz et al., 2001; Wei et al., 2006c). Diamondoids are more thermally stable than most other hydrocarbons (Dahl et al., 1999) and are significantly more resistant to biodegradation (Williams et al., 1986; Wingert, 1992; Grice et al., 2000). Therefore, diamondoids are commonly utilized to determine the thermal maturity of highly mature source rocks and crude oils (Chen et al., 1996; Li et al., 2000; Zhang et al., 2005), estimate the extent of oil cracking (Dahl et al., 1999), and evaluate biodegradation of crude oil (Grice et al., 2000; Wei et al., 2007a).

Although diamondoid indices are used routinely in different aspects of petroleum geochemistry, the formation and evolution of diamondoids in source rocks are not well understood. Diamondoids are derived from the pyrolysis of different source matters that include immature sedimentary rock (Wei et al., 2006c, 2007c), peat (Wei et al., 2007b), kerogens (Gordadze, 2002; Fang et al., 2015b), coal (Fang et al., 2015a), crude oil (Fang et al., 2012), different fractions of crude oil (Fang et al., 2013), and single *n*-alkanes (Gordadze and Giruts, 2008). These studies confirmed the importance of thermal maturation on the formation and evolution of diamondoids. And oil cracking experiments documented that diamondoids experience successive stages of generation, accumulation, and degradation with increasing thermal maturity (Fang et al., 2012). The catalytic effect of minerals on the formation of diamondoids has been studied using a series of simulation experiments and the results suggest that different types of minerals have distinct effects on the generation of diamondoids (Wei et al., 2006a, 2006c).

Organic matter in source rocks includes soluble (bitumen) and insoluble (kerogen) components (Burnham and Braun, 1990). The extractable

ARTICLE IN PRESS

W. Jiang et al.   Marine and Petroleum Geology xxx (xxxx) xxx–xxx

bitumen in source rocks is the main component to create diamondoids during thermal maturation based on the results of simulation experiments (Fang et al., 2015b). Li et al. (2015) documented that lower diamondoids formed during the thermal maturation stage of source rocks are derived mainly from the secondary cracking of bitumen and not by the primary cracking of kerogens. However, bitumen is derived from kerogen during thermal maturation and the ability to generate bitumen is a function of the type of kerogen. Therefore, the type of a source rock can possibly be an important factor that determines its ability to generate diamondoids.

Studies on natural samples have documented the effect of different types of organic matters on the generation and distribution of diamondoids. Wei et al. (2006b) proposed that the abundance of diamondoids in organic-rich sedimentary rocks is greater, by an order of magnitude, compared with diamondoids in coal at the same maturity level. Differences are also noted in the distribution of diamondoids in other source rocks (Schulz et al., 2001).

The study of natural samples must account for differences in maturity, lithology, and depositional environment. It is also difficult to obtain a group of natural samples that have the same source, but represent a wide range in thermal maturity. Therefore, thermal simulation experiments are often conducted to study the potential effects of single parameters, meanwhile, exclude other factors. The present study conducted thermal simulation experiments on kerogens in three source rocks (e.g., Type I shale, Type II$_A$ shale, and Type III coal) to investigate the effect of different organic matters on the generation and evolution of thermogenic diamondoids by comparing similarities and differences in diamondoid yields and diamondoid indices during thermal maturation of source rocks.

2. Samples and methods

2.1. Samples

Sample descriptions and geochemical data are presented in Table 1. Sample A is an oil shale with total organic carbon (TOC) of 20.3 wt% from the Eocene–Oligocene Youganwo Formation in the Maoming Basin that contains high concentrations of Type I kerogen and has a low maturity (Table 1). Sample B is an immature shale with vitrinite reflectance (Ro) of 0.35% from the Oligocene Dongying Formation in the Bohai Bay Basin that contains Type II$_A$ kerogen and has TOC = 2.2 wt% (Table 1). Type II$_A$ organic matter type is a sapropel-humic mixed type (a subclass of type II) that the content of sapropel is more abundant than humic, which was suggested by Yang et al. (1982) based on the study of Chinese source rocks and was widely used in petroleum geology in China. Sample C is a semi-clarain of low-grade incoalation from the Paleocene Lijiaya Formation in the Bohai Bay Basin, and the Ro data indicate the coal is immature (Table 1).

2.2. Extraction of source rocks

Samples were cleaned using dichloromethane, ground, and sieved with a 100-mesh screen. A Soxhlet-extraction using mixed dichloromethane and methanol solvent (dichloromethane:methanol = 93:7, v/v) was performed on each aliquot of sample for 72 h. These extracts were rotary evaporated and placed in 2 mL sample vials for diamondoid analysis.

2.3. Pyrolysis experiments

The samples of ground shale and coal were demineralized using hydrochloric and hydrofluoric acids to isolate kerogen. The kerogen concentrates were ground and sieved with a 100-mesh screen. A Soxhlet-extraction using dichloromethane:methanol (93:7 v/v) was performed for 72 h to remove traces of free hydrocarbons potentially bound in the kerogen matrix. The extracted kerogens were then dried at 50 °C for 12 h.

Pyrolysis experiments involving three types of kerogen (e.g., Type I, II$_A$, and III; Table 1) were performed in sealed gold tubes after the method of Fang et al. (2012). The individual tubes were 40 mm long, with an inner diameter of 4.2 mm and 0.25 mm thick walls. Aliquots of each type of kerogen weighing 15–50 mg were loaded into the tubes and purged with argon for 10 min, before being sealed under an argon atmosphere. A pair of sealed tubes containing a specific type of kerogen was then placed in a stainless steel autoclave. Different series of samples were heated at two constant rates of 20 °C/h and 2 °C/h, respectively, under a constant pressure of 50 MPa. Samples were heated to a specific temperature and then removed from the autoclave to provide data between 330 °C and 595 °C. A total of 12 samples were analyzed for each heating rate. The thermal maturation of samples was calculated using the Easy%Ro method developed by Sweeney and Burnham (1990).

2.4. Analysis of pyrolytic products

Each pair of gold tubes for a specific type of kerogen and temperature point was analyzed using different methods to determine the composition of hydrocarbons and diamondoid. The method of Li et al. (2015) was used to identify gaseous hydrocarbons. Prior to analysis, individual gold tubes were weighed using a Sartorius CPA225D electronic balance accurate to 0.01 mg per 100 g. A tube was cleaned using dichloromethane and then placed in a glass vacuum system connected to the inlet of a gas chromatograph (GC). A steel needle was used to pierce the tube and the chemical compositions of gaseous hydrocarbons were determined by an Agilent 6890B GC modified by Wasson ECE Instrument, as described by Pan et al. (2006). Results were quantified using an external standard method.

Following GC analysis, the pierced gold tube was dried at 50 °C in an electric vacuum–drying oven to evaporate gasoline hydrocarbons. The drying continued until weights determined for the tube remained constant. The difference in weight of the tube after analysis is considered to be the total amount of inorganic gaseous compounds, gaseous hydrocarbons, and light hydrocarbons (LHs) generated from kerogen. Therefore, the yield of LHs is obtained by subtracting organic and inorganic gaseous compounds from the weight difference in the tube pre- and post-analysis.

After having determined the LHs mass, the gold tube was cut in half and placed in a 4 mL sample vial filled with dichloromethane. The vial was treated ultrasonically for 30 min to dissolve any heavy hydrocarbons (HHs) in the gold tube that formed from kerogen, and then the vial was left undisturbed for 12 h. The resulting solution was filtered and then evaporated using a stream of nitrogen gas to obtain a concentrate of HHs. This concentrate was weighed using the Sartorius

Table 1
Geochemical data of the samples used in the simulation experiments.

Sample	Lithology	Location	Formation	Age	TOC (wt %)	Ro (%)	Tmax (°C)	S$_1$ (mg/ g)	S$_2$ (mg/g)	HI (mg/ gTOC)	Type of kerogen
A	Shale	Maoming Basin, SouthChina	Youganwo	Eocene -Oligocene	20.3	0.41	423	2.3	97.54	480	I
B	Shale	Bohai Bay Basin, NorthChina	Dongying	Oligocene	2.2	0.35	427	4.18	10.86	503	II$_A$
C	Coal	Bohai Bay Basin, NorthChina	Lijiaya	Palaeocene	59.7	0.40	429	1.21	48.51	91	III

CPA225D electronic balance.

Diamondoid analysis of the second gold tube in each pair began with immersion in liquid nitrogen for 25–30 min. A rapid succession of events followed with the tube being cut in half and placed in a 4 mL sample vial filled with isooctane. Then a 50 μL internal standard solution of n-dodecane-d_{26} and n-hexadecane-d_{34} in isooctane was injected into the sample vial. After 10 min of ultrasonic treatment to dissolve any analytes, the vial was placed in a centrifuge for 10 min to precipitate asphaltenes. The resulting supernatant was transferred to a 2 mL vial for diamondoid analysis. The diamondoids were identified and measured using gas chromatography-triple quadrupole mass spectrometry (GC–MS–MS), according to the method of Liang et al. (2012).

3. Results and discussion

3.1. Generation and decomposition of hydrocarbons during thermal maturation

The yields of pyrolytic products were normalized to TOC to eliminate the difference of the organic matter content in kerogens; i.e. we determined the mass of pyrolytic products at a given maturity level relative to the mass of TOC in the kerogen samples (in mg/g TOC). And the yield percentages of the products were determined by normalizing their corresponding yields to the total yields of the products (in wt.% TOC). Pyrolytic products include methane, C_2–C_5 gaseous hydrocarbons (GHs), C_6–C_{12} LHs, and C_{13+} HHs. The data presented in Fig. 1 show the percentages of different hydrocarbons generated during thermal maturation of the three types of kerogen. The total hydrocarbon conversion rate of kerogen in Fig. 1 reaches a maximum at ca. 1.0% EasyRo
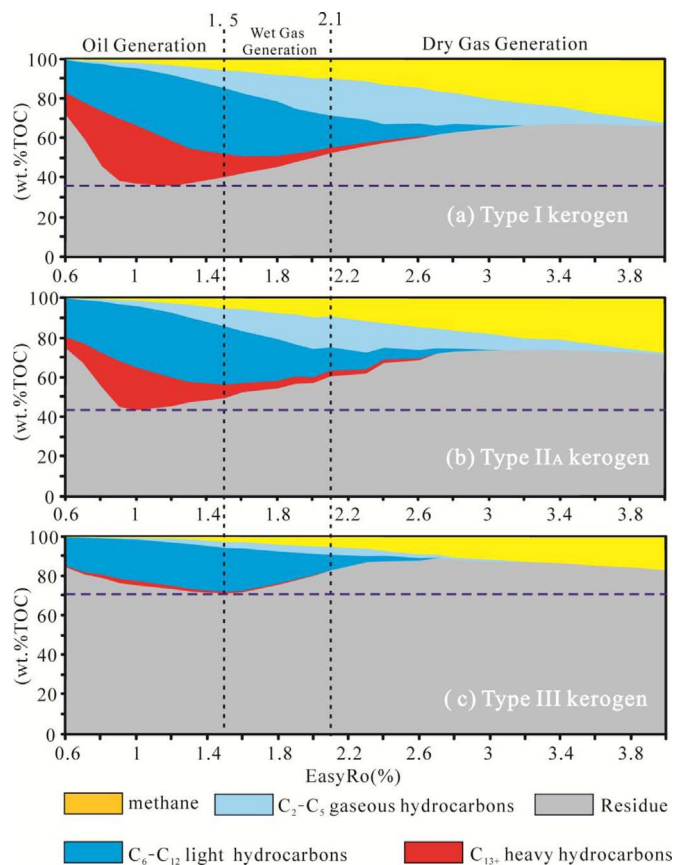

Fig. 1. The percentage of different components (e.g., methane, C_2–C_5 gaseous hydrocarbons (GHs), C_6–C_{12} light hydrocarbons (LHs), C_{13+} heavy hydrocarbons (HHs), and residue) versus EasyRo (%) for the pyrolysis experiments of kerogens. The C_2–C_5 GHs include C_2, C_3, i-C_4, n-C_4, i-C_5, and n-C_5 alkanes; the LHs are C_6–C_{12} n-alkanes; and the HHs are C_{13+} fractions.

(Types I and II_A kerogens) and at ca. 1.5% EasyRo (Type III kerogen), decreases gradually to 2.8% EasyRo, and then remains constant for Types I and II_A kerogen but increases gradually for Type III kerogen. The simulation experiments have maximum total hydrocarbon yields of 63.5% (Type I), 56.7% (Type II_A), and 28.8% (Type III; Fig. 1).

The cracking process of the different kerogens is divided into three stages: oil generation (0.6%–1.5% EasyRo), wet-gas generation (1.5%–2.1% EasyRo), and dry-gas generation (> 2.1% EasyRo). The methane yield of the three kerogen types increases continuously throughout the simulation experiment (e.g., 0.6%–4.0% EasyRo). However, the maximum yields of methane are highest for Type I (32.1%) and lowest for Type III (17.4%; Fig. 1). In the oil generation stage (0.6%–1.5% EasyRo), the yield of C_{13+} HHs gradually increases for the different types of kerogen to reach maximum values at ~1.0% EasyRo. These maxima are 32.5% (Type I), 23.3% (Type II_A), and 1.4% (Type III; Fig. 1). Further thermal maturation results in a decrease of values due to the decomposition of C_{13+} HHs. The generation of C_{13+} HHs by coal is less than the other samples because coal contains high concentrations of polycyclic aromatic hydrocarbons, but has low concentrations of long straight-chain hydrocarbons (Wei et al., 2006b). In this stage of oil generation, the yield of C_6–C_{12} LHs increases gradually to 1.5% EasyRo, where the maximum LH yields are 35.2% (Type I), 33.0% (Type II_A), and 23.3% (Type III; Fig. 1).

The cracking of kerogen then enters into the wet-gas generation stage (1.5%–2.1% EasyRo). The C_{13+} HHs decompose continuously and the yield of C_6–C_{12} LHs begins to decrease, but the yield of C_2–C_5 GHs increases rapidly to reach a maximum at ~2.1% EasyRo (Fig. 1). The maximum yields of C_2–C_5 gaseous hydrocarbons are 19.7% (Type I), 15.9% (Type II_A), and 3.3% (Type III; Fig. 1). As coal generated low amounts of C_{13+} HH, this is also the case for C_2–C_5 gaseous hydrocarbons. The cracking of kerogen enters into the dry-gas generation stage at 2.1% EasyRo. All fractions crack into methane and solid residue, with C_2–C_5 gaseous hydrocarbons being the main source of methane for Type I and II_A kerogens.

3.2. Yields of diamondoids

The same process of normalizing yields of pyrolytic products is used to assess the evolution of diamondoids during the maturation of kerogens, with values of TOC reported in μg/g TOC. The data presented in Fig. 2 show the yields of total adamantanes and diamantanes during kerogen pyrolysis. Adamantanes and diamantanes are terms that refer to 22 adamantane compounds and 10 diamantane compounds, respectively, which are listed in Appendix 1.

Experimental results indicate that diamondoids have formed when kerogens enter the oil window (Fig. 2a). The initial yields of adamantanes in Type I, II_A, and III kerogens are 5.2, 4.2, and 1.2 μg/g TOC at 0.6% EasyRo (Fig. 2a), respectively. With increasing maturation, the yield of adamantanes in Type I kerogen rises rapidly to reach a maximum of 85.3 μg/g TOC at the end of the wet-gas generation stage (2.1% EasyRo; Fig. 2a). The yield of adamantanes decreases entering the dry-gas generation stage, which reflects the decomposition of adamantanes. This decomposition continues and is nearly complete when the maturity exceeds 3.0% EasyRo.

The evolution of adamantanes produced from Type II_A and III kerogens follows a similar trend to that of Type I kerogen. Adamantanes have formed when kerogens enter the oil window and the yield rises continuously to reach a maximum at the end of the wet-gas generation stage (Fig. 2a). The decomposition of adamantanes generated from Type II_A and III kerogens occurs in the dry-gas generation stage.

Although the evolutionary trends of adamantanes produced from Type I, II_A, and III kerogens are similar, the actual yields are different. The maximum yield of adamantanes is 85.3, 104.7, and 19.6 μg/g TOC for kerogen Types I, II_A, and III (Fig. 2a), respectively. These data reflect the potential of different source rocks to generate hydrocarbons. The concentrations of HIs are 480, 503, and 91 mg/g TOC for kerogen Types
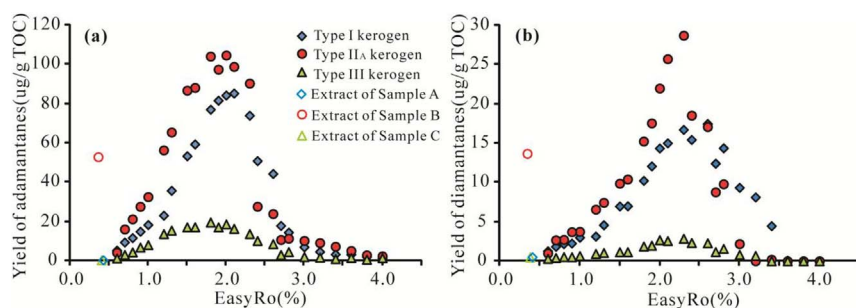
Fig. 2. Plots showing the yield (µg/g TOC) of (a) adamantanes and (b) diamantanes vs. EasyRo (%) for the pyrolysis experiments of kerogens.

I, II_A, and III (Table 1), respectively. The maximum yield of adamantanes in source rocks seems to be related to the hydrocarbon-generation potential of source rocks, as the concentration of HIs in Type I and II_A kerogens is more than five times that of Type III kerogen and the maximum yield of adamantanes in Type I and II_A kerogens is roughly five times greater than in Type III kerogen.

The data presented in Fig. 2 show that the three types of kerogen produce lower yields of diamantanes compared with adamantanes. The yields of diamantanes increase dramatically in the late oil generation to early dry-gas generation stages (1.0%–2.3% EasyRo), with maximum values of 17.5 and 28.7 µg/g TOC for kerogen Types I and II_A (Fig. 2b), respectively. The maximum yields of diamantanes occur at a higher thermal maturity than those of adamantanes, as does the onset of decomposition, e.g., Fig. 2 shows that the maximum yield of adamantanes in Type I kerogen occurs at 2.1% EasyRo, which is lower than the 2.3% EasyRo for diamantanes. In contrast, diamantanes in Type III kerogen are barely detectable and the maximum yield is only 2.8 µg/g TOC (Fig. 2b).

The results of Li et al. (2015) established that lower diamondoids are derived mainly from the secondary cracking of bitumen, and an upper limit of maturity for the generation of diamondoids from kerogens occurs at 1.3% EasyRo. Therefore, diamondoids generated above 1.3% EasyRo in the present study are derived from the secondary cracking of bitumen. Fig. 2a shows that > 60% of the peak yields of adamantanes in Type I and II_A kerogens are generated by the secondary cracking of bitumen (1.3%–2.1% EasyRo) and < 40% is due to the primary cracking of kerogens (0.6%–1.3% EasyRo). In contrast, adamantanes in Type III kerogen have > 80% of the peak yield being generated by the primary cracking of kerogen and only a small contribution from the secondary cracking of bitumen. This is consistent with that Type III kerogen has a much lower potential to generate HHs than Type I and II_A kerogens, which could account for the low yield of diamondoids in Type III kerogen during the pyrolysis experiments.

In summary, the evolution of thermogenic lower diamondoids in the three types of kerogen is similar, with the formation of diamondoids occurring during the oil window and the wet-gas generation stage and the degradation happening during the dry gas stage. However, the yield of diamondoids is related to the type of kerogen. Thermogenic diamondoids in Type I and II_A kerogens form mainly by the secondary cracking of bitumen. In contrast, diamondoids in Type III kerogen form mainly by the primary cracking of kerogens, because Type III kerogen has a much lower potential to generate HHs than Type I and II_A kerogens. This is illustrated by the data in Fig. 2 that show how diamondoid generation in Type I or II_A kerogens is four to five times higher than in Type III kerogen. Another difference is that diamondoids derived from Type III kerogen are dominated by adamantanes that at the generation stage of diamondoids, the ratio of adamantanes/diamondoids (As/Ds) in Type III kerogen is obviously bigger than those in Type I and II_A kerogens (Fig. 3d in section 3.3.1). These results indicate that the formation and content of lower diamondoids is affected by the type of organic matter in source rocks.

3.3. Diamondoid indices

The diamondoid indices that are currently used include concentration and isomerization ratios, which are applicable under certain conditions. Fang et al. (2013) showed that the concentration-related diamondoid maturity parameters are suitable for a relatively lower maturity level while the isomerization-related diamondoid maturity parameters are available for the higher maturity level. Li et al. (2000) proposed that the methyl diamantane index (MDI) may have limited applicability in very mature sections (Ro > 2.0%). In order to better understand the effect of organic matter on the generation and evolution of diamondoids in source rocks, it is necessary to study comparatively the variations in two kinds of diamondoid indices during the thermal maturation of different kerogens.

3.3.1. Concentration ratios

Fang et al. (2013) proposed that the concentration ratio of diamondoid groups in nature is equal to the yield ratio of the corresponding diamondoid groups. Therefore, it is possible to calculate concentration ratios by measuring the yields of the corresponding diamondoids during pyrolysis experiments conducted in the present study. Specific concentration ratios of methyladamantanes/methyldiamantanes (MAs/MDs), dimethyladamantanes/methyldiamantanes (DMAs/MDs), dimethyladamantanes/dimethyldiamantanes (DMAs/DMDs), and adamantanes/diamantanes (As/Ds) were calculated to assess the evolution of diamondoids in different kerogens during thermal maturation. The data presented in Fig. 3 show that these concentration ratios for the three types of kerogen have very similar evolutionary trends. The general trend begins with a sharp rise in the oil generation stage (0.6% EasyRo) that peaks in the wet-gas generation stage (1.5% EasyRo). A sharp initial drop in the wet-gas and dry-gas generation stages becomes more gradual at ~2.5% EasyRo (Fig. 3).

Although concentration ratios of three types of kerogen follow a general trend with thermal maturation, there are obvious differences between Type III kerogen and Type I or II_A kerogen in the range of 1.0–2.0% EasyRo. The greatest spread in data occurs at 1.5% EasyRo and values of MAs/MDs are 3.5 (Type I), 3.1 (Type II_A), and 6.2 (Type III; Fig. 3). This difference in values results from the low yields of diamantanes for Type III kerogen. Such disparities in the data allow different types of organic matters to be distinguished using concentration ratios in the range of 1.0%–2.0% EasyRo.

As indicated above, concentration ratios have a non-monotonic relationship with EasyRo during the whole thermal maturation process, the obvious peak in the evolutionary trend of the concentration ratio suggests that a certain concentration ratio correlate with two different maturities in the ascending and descending legs. A way to validate the different maturities is by determining the general maturation stage of the source rocks using other maturity indices. As relatively large quantification errors result from the low concentrations of diamondoids at diamondoid destruction stage, it is appropriate to use concentration ratios in combination with other geological or geochemical data to determine the thermal maturities of source rocks within the oil generation stage (1.0–1.5% EasyRo).
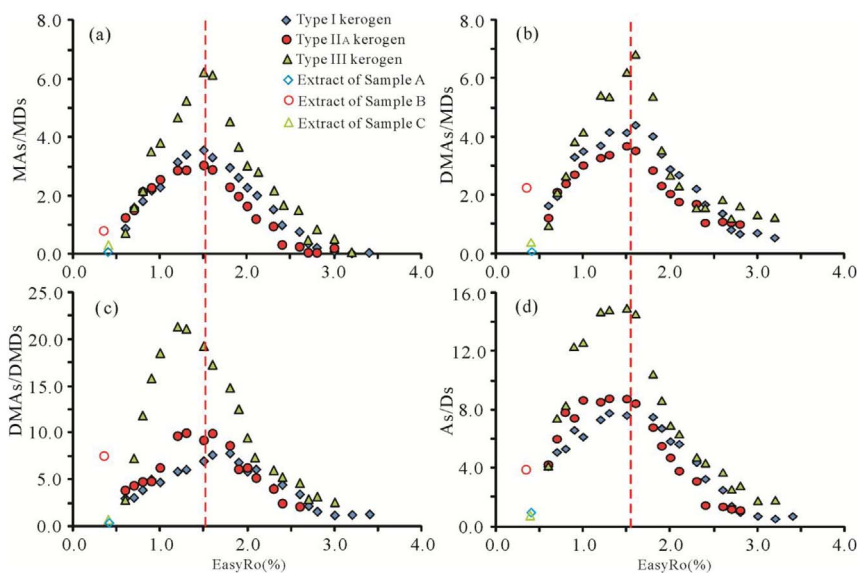
Fig. 3. Plots of concentration ratios of diamondoids vs. EasyRo (%) for the pyrolysis experiments of kerogens. The different concentration ratios are (a) MAs/MDs, (b) DMAs/MDs, (c) DMAs/DMDs, and (d) As/Ds.

3.3.2. Isomerization ratios

Diamondoid compounds that contain a greater degree of substitution by bridgehead carbons are more stable in a thermodynamic sense (Clark et al., 1979; Wingert, 1992; Wei et al., 2007b). Fang et al. (2015b) documented that isomers containing a greater degree of substitution by bridgehead carbons (e.g., 1,3-DMA, 1,3,5-TMA, 4-MD, and 4,9-DMD) increase in abundance more than other isomers during source rock maturation. Therefore, isomerization indices of diamondoids are used to assess the thermal maturity of crude oil and source rocks (Chen et al., 1996; Li et al., 2000; Zhang et al., 2005). There are nine isomerization indices: MAI [1-MA/(1-MA + 2-MA)]; EAI [1-EA/(1-EA + 2-EA)]; DMAI-1 [1,3-DMA/(1,3-DMA + 1,2-DMA)]; DMAI-2 [1,3-DMA/(1,3-DMA + 1,4-DMA)]; TMAI-1 [1,3,5-TMA/(1,3,5-TMA + 1,3,4-TMA)]; TMAI-2 [1,3,5-TMAI/(1,3,5-TMA + 1,3,6-TMA)]; MDI [4-MD/(4-MD + 1-MD + 3-MD)]; DMDI-1 [4,9-DMD/(4,9-DMD + 3,4-DMD)]; and DMDI-2 [4,9-DMD/(4,9-DMD + 4,8-DMD)] (Chen et al., 1996; Grice et al., 2000; Schulz et al., 2001; Zhang et al., 2005; Wei et al., 2007b; Fang et al., 2012, 2013).

The data presented in Fig. 4 show the variations of diamondoid isomerization indices during thermal maturation of different kerogens. Evolutionary trends are very similar for isomerization ratios of the three kerogens, especially when the maturity is < 1.3% EasyRo (Fig. 4). These data are consistent with Schulz et al. (2001) and indicates that the aimed diamondoid indices (e.g., MAI and EAI) are virtually unaffected by increasing maturity within the oil window. However, the overlap in values of isomerization ratios for the three kerogens in this stage makes it impossible to distinguish source rocks.

Above 1.3% EasyRo, the isomerization indices increase rapidly and have a near linear correlation with EasyRo (Fig. 4). Isomerization indices that correlate well with EasyRo over restricted ranges in the present study are: MAI (1.3%–2.8% EasyRo), EAI (1.3%–2.8% EasyRo), DMAI-1 (1.6%–2.8% EasyRo), DMAI-2 (1.6%–2.8% EasyRo), TMAI-1 (1.8%–3.0% EasyRo), TMAI-2 (1.8%–3.0% EasyRo), MDI (2.1%–3.2% EasyRo), and DMDI-1 (2.1%–3.2% EasyRo, Fig. 4). Therefore, these isomerization indices can be used to evaluate the maturity of source rocks at relatively high levels of maturity.

Based on the work of Fang et al. (2013, 2015a, 2015b), plots of DMAs/MDs vs. DMAI-1 and DMAs/MDs vs. TMAI-1 were constructed to assess the maturity of crude oil and source rocks over a wider range of maturity. Data for DMAs/MDs and DMAI-1 plot within area A at a low level of maturity (< 1.0% EasyRo; Fig. 5a). Between 1.0% and 1.5% EasyRo, index values shift toward area B (B₁, B₂ and B₃ for Type I, IIₐ and III kerogens, respectively), with DMAs/MDs values increasing rapidly from a base of ~1.0 up to 4.4 (Type I), 3.7 (Type IIₐ), and 7.1

(Type III) while the values of DMAI-1 having little variation between 1.0% and 1.5% EasyRo (Fig. 5a). At higher levels of maturity (1.5%–3.0% EasyRo) the index values shift to area C (Fig. 5a), with DMAs/MDs values decreasing to zero and DMAI-1 values increasing to one. The data of DMAs/MDs and TMAI-1 show very similar evolutionary trends for the three kerogens with increasing maturity (Fig. 5b).

Although the evolutionary trends in Fig. 5 are quite similar, differences in the position of area B (e.g., B₁, B₂, and B₃) are evident for Type I, IIₐ, and III kerogens during the pyrolysis experiments. Fang et al. (2015a) documented that the evaporation of oil prior to pyrolysis did not change the evolutionary trends of DMAs/MDs vs. DMAI-1 or DMAs/MDs vs. TMAI-1 during the oil cracking process, but caused the evolutionary trends to integrally shift downward and to the left, compared with the original oil sample. Therefore, the concentration of volatile components in diamondoid-generation precursors could possibly affect the distribution of diamondoids in plots of DMAs/MDs vs. DMAI-1 and DMAs/MDs vs. TMAI-1. The relative content of volatile components (e.g., LHs) generated from Type III kerogen is higher compared with Type I and IIₐ kerogens in the oil-generation stage. Therefore, differences in the type of organic matter can account for the different locations of B₁, B₂, and B₃ in Fig. 5. This not only allows the DMAs/MDs vs. DMAI-1 and DMAs/MDs vs. TMAI-1 plots to be used in determining the maturity of source rocks and crude oil over a wide EasyRo range (1.0%–3.0%), but also to distinguish sources of organic matter for oils by determining the location of area B, especially to differentiate the type III one from the type I and IIₐ ones.

3.4. Diamondoids in the extracts of different source rocks

The amounts of diamondoid in the extracts of the three source rocks (e.g., Samples A, B, and C) were quantified and normalized to the TOC content (in μg/g TOC) as we stated earlier. Data in Fig. 2 indicate that diamondoids already existed in immature source rocks. Samples A and C are oil shale and coal, respectively, which contain very low amounts of diamondoids. Sample B is an immature shale and contains significantly more diamondoids (Fig. 2). Therefore, diamondoids could be generated during diagenesis as proposed by Wei et al. (2007b), with the yield of diamondoids reflecting differences in the type of organic matter in source rocks.

The composition and distribution of diamondoids in the extracts of the three source rocks have also been analyzed. The values of concentration ratios for Sample B are significantly higher than for Samples A and C (Fig. 3), but the values for Samples A and C are very similar. These relationships suggest that the concentration ratios of diamondoids in immature source rocks can distinguish Type IIₐ source rocks
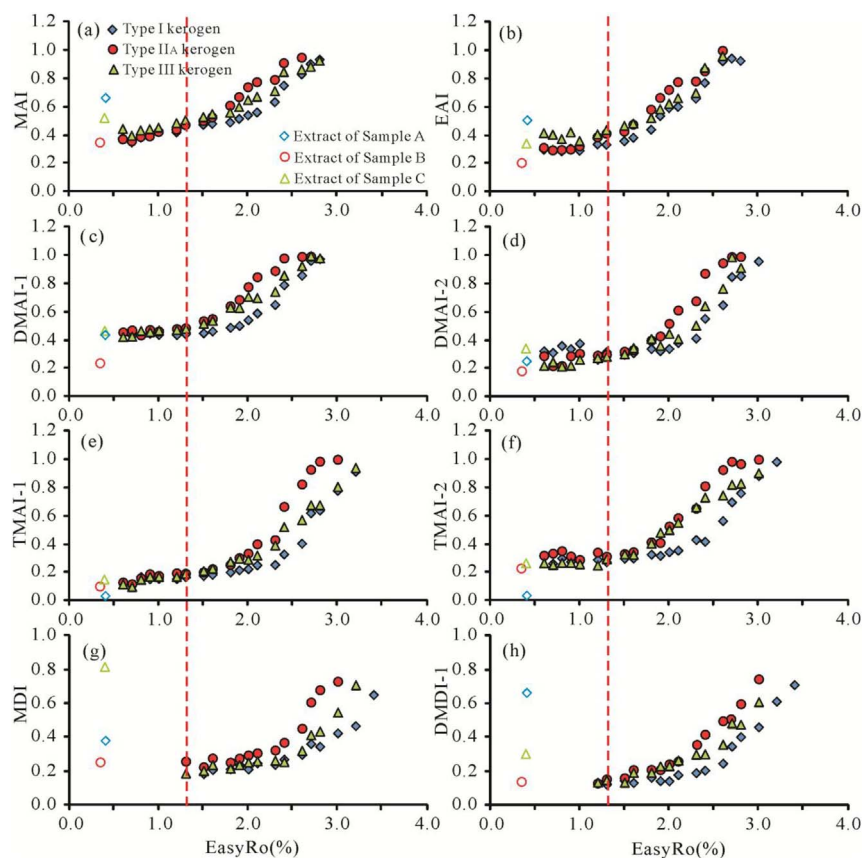
Fig. 4. Plots of diamondoid isomerization indices vs. EasyRo (%). The different isomerization ratios are (a) MAI, (b) EAI, (c) DMAI-1, (d) DMAI-2, (e) TMAI-1, (f) TMAI-2, (g) MDI, and (h) DMDI-1.

from Type I and III source rocks. Additionally, the concentration ratios in the extracts are distinct from those at the point when kerogen began to degrade. The values of concentration ratios in Samples A and C are much lower than at the point where kerogen started to crack (~0.6% EasyRo) (Fig. 3). In contrast, the concentration ratios in Sample B have higher values than at the point where kerogen started to crack, except for the As/Ds index (Fig. 3d). These results indicate that the mechanism of diamondoid formation during diagenesis is different than for thermogenic diamondoids created during kerogen pyrolysis.

The data in Fig. 4 show that there are considerable differences between diamondoid isomerization indices (e.g., MAI, EAI, MDI, and DMDI-1) of the three source rock extracts. Yet isomerization indices are not affected by thermal maturity at diagenetic stage. Therefore, the different data reflect differences in the three source rocks and this validates using isomerization indices of the extracts to identify the type of source rock. As the composition and distribution of diamondoids formed during diagenesis are distinct for different types of rocks, the potential exists to use diamondoid indices of immature rocks to determine the type of source rock.

4. Conclusions

Three types of kerogen were used to investigate the effect different organic matters have on the formation and evolution of lower diamondoids (e.g., adamantanes and diamantanes). Important results and conclusions are:

1) The lower diamondoids in Type I, II_A, and III kerogens mainly form within the oil generation and wet-gas generation stages (0.6%–2.1% EasyRo for adamantanes and 1.0%–2.3% EasyRo for diamantanes) and decompose during the dry-gas generation stage (EasyRo > 2.1% for adamantanes and EasyRo > 2.3% for diamantanes).
2) Thermogenic diamondoids in Type I and II_A kerogens mainly form by the secondary cracking of bitumen, whereas the primary cracking of kerogens is important in diamondoid formation in Type III kerogen due to its lower potential to generate heavy hydrocarbons. The maximum yields of diamondoids from Type I and II_A kerogens are about five times that of Type III kerogen, but Type III kerogen produces relatively more adamantanes than diamantanes.
3) Concentration ratios of diamondoids can be used as both maturity indices for source rocks of relatively low maturity (1.0%–1.5%
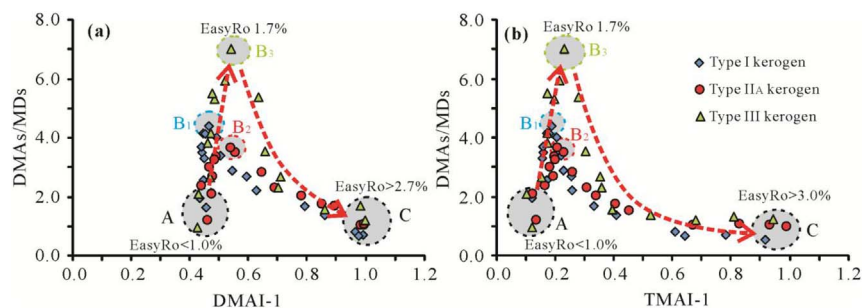

Fig. 5. Plots of (a) DMAs/MDs vs. DMAI-1 and (b) DMAs/MDs vs. TMAI-1 for the pyrolysis experiments of kerogens.

EasyRo) and to distinguish the type of source rock between 1.0% and 2.0% EasyRo. Isomerization ratios are better maturity indices at higher maturity stages (> 1.3% EasyRo) and are not affected by the type of kerogen. The plots of DMAs/MDs vs. DMAI-1 and DMAs/MDs vs. TMAI-1 can be used to evaluate the maturity of source rocks over a wider EasyRo range (1.0%–3.0% EasyRo) and distinguish types of organic matters.

4) Diamondoids formed during diagenesis have different concentrations and distributions in different types of source rocks. This could allow diamondoid indices of immature source rocks to be used to identify the type of source rock.

Acknowledgements

Appendix 1. The names and abbreviations of diamondoid compounds referenced in this study

Compound no.	Molecular formula	Diamondoid compound	abbreviation
1	$C_{10}H_{16}$	Adamantane	A
2	$C_{11}H_{18}$	1-Methyladamantane	1-MA
3	$C_{12}H_{20}$	1,3-Dimethyladamantane	1,3-DMA
4	$C_{13}H_{22}$	1,3,5-Trimethyladamantane	1,3,5-TMA
5	$C_{14}H_{24}$	1,3,5,7-Tetramethyladamantane	1,3,5,7-TeMA
6	$C_{11}H_{18}$	2-Methyladamantane	2-MA
7	$C_{12}H_{20}$	1,4-Dimethyladamantane(cis)	1,4-DMA(*cis*)
8	$C_{12}H_{20}$	1,4-Dimethyladamantane(trans)	1,4-DMA(*trans*)
9	$C_{13}H_{22}$	1,3,6-Trimethyladamantane	1,3,6-TMA
10	$C_{12}H_{20}$	1,2-Dimethyladamantane	1,2-DMA
11	$C_{13}H_{22}$	1,3,4-Trimethyladamantane(cis)	1,3,4-TMA(*cis*)
12	$C_{13}H_{22}$	1,3,4-Trimethyladamantane(trans)	1,3,4-TMA(*trans*)
13	$C_{14}H_{24}$	1,2,5,7-Tetramethyladamantane	1,2,5,7-TeMA
14	$C_{12}H_{20}$	1-Ethyladamantane	1-EA
15	$C_{12}H_{20}$	2,6- + 2,4-Dimethyladamantane	2,6- + 2,4-DMA
16	$C_{13}H_{22}$	1-Ethyl-3-methyladamantane	1-E − 3-MA
17	$C_{13}H_{22}$	1,2,3-Trimethyladamantane	1,2,3-TMA
18	$C_{14}H_{24}$	1-Ethyl-3,5-dimethyladamantane	1-E − 3,5-DMA
19	$C_{12}H_{20}$	2-Ethyladamantane	2-EA
20	$C_{14}H_{24}$	1,3,5,6-Tetramethyladamantane	1,3,5,6-TeMA

References

Burnham, A.K., Braun, R.L., 1990. Development of detailed model of petroleum formation, destruction, and expulsion from lacustrine and marine source rocks. Org. Geochem 16, 27–39.

Chen, J.H., Fu, J.M., Sheng, G.Y., Liu, D.H., Zhang, J.J., 1996. Diamondoid hydrocarbon ratios: novel maturity indices for highly mature crude oils. Org. Geochem 25, 179–190.

Clark, T., Knox, T.M., McKervey, M.A., Mackle, H., Rooney, J.J., 1979. Thermochemistry of bridgehead-ring substances. Enthalpies of formation of some diamondoid hydrocarbons and perhydroquinacene-comparisons with data from empirical force field calculations. J. Am. Chem. Soc. 101, 2404–2410.

Dahl, J.E., Moldowan, J.M., Peters, K., Claypool, G., Rooney, M., Michael, G., Mello, M., Kohnen, M., 1999. Diamondoid hydrocarbons as indicators of oil cracking. Nature 399, 54–56.

Fang, C.C., Wu, W., Liu, D., Liu, J.Z., 2015a. Evolution characteristic and application of diamondoids in coal measures. Nat. Gas. Geosci. 26, 110–117 (in Chinese with English abstract).

Fang, C.C., Xiong, Y.Q., Li, Y., Liu, J.Z., 2013. The origin and evolution of adamantanes and diamantanes in petroleum. Geochim. Cosmochim. Acta 120, 109–120.

Fang, C.C., Xiong, Y.Q., Li, Y., Chen, Y., Tang, Y.J., 2015b. Generation and evolution of diamondoids in source rock. Mar. Pet. Geol. 67, 197–203.

Fang, C.C., Xiong, Y.Q., Liang, Q.Y., Li, Y., 2012. Variation in abundance and distribution of diamondoids during oil cracking. Org. Geochem 47, 1–8.

Grice, K., Alexander, R., Kagi, R.I., 2000. Diamondoid hydrocarbon ratios as indicators of biodegradation in Australian crude oils. Org. Geochem 31, 67–73.

Gordadze, G.N., 2002. Themolysis of Organic Matter in Oil-and-Gas Exploratory Geochemistry. Inst. Geol. Razrab. Goryuch. Iskop, Moscow, in Russian.

Gordadze, G.N., Giruts, M.V., 2008. Synthesis of adamantane and diamantane hydrocarbons by high-temperature cracking of higher n-alkanes. Pet. Chem. 48, 414–419.

Landa, S., Machacek, V., 1933. Adamantane, a new hydrocarbon extracted from petroleum. Collect. Czech. Chem. Commun. 5, 1–5.

Li, J.G., Philp, P., Cui, M.Z., 2000. Methyl diamantane index (MDI) as a maturity parameter for Lower Palaeozoic carbonate rocks at high maturity and overmaturity. Org. Geochem 31, 267–272.

Li, Y., Chen, Y., Xiong, Y.Q., Wang, X.T., Fang, C.C., Zhang, L., Li, J.H., 2015. Origin of adamantanes and diamantanes in marine source rock. Energy fuels. 29, 8188–8194.

Liang, Q.Y., Xiong, Y.Q., Fang, C.C., Li, Y., 2012. Quantitative analysis of diamondoids in crude oils using gas chromatography-triple quadrupole mass spectrometry. Org. Geochem 43, 83–91.

Pan, C.C., Yu, L.P., Liu, J.Z., Fu, J.M., 2006. Chemical and carbon isotopic fractionations of gaseous hydrocarbons during abiogenic oxidation. Earth Planet. Sci. Lett. 246, 70–89.

Schulz, L.K., Wilhelms, A., Rein, E., Steen, A.S., 2001. Application of diamondoids to distinguish source rock facies. Org. Geochem 32, 365–375.

Sweeney, J.J., Burnham, A.K., 1990. Evaluation of a simple model of vitrinite reflectance based on chemical-kinetics. Am. Assoc. Pet. Geol. Bull. 74, 1559–1570.

Wei, Z.B., Moldowan, J.M., Dahl, J., Goldstein, T.P., Jarvie, D.M., 2006a. The catalytic effects of minerals on the formation of diamondoids from kerogen macromolecules. Org. Geochem 37, 1421–1436.

Wei, Z.B., Moldowan, J.M., Jarvie, D.M., Hill, R., 2006b. The fate of diamondoids in coals and sedimentary rocks. Geology 34, 1013–1016.

Wei, Z.B., Moldowan, J.M., Paytan, A., 2006c. Diamondoids and molecularbiomarkers generated from modern sediments in the absence and presence of minerals during hydrous pyrolysis. Org. Geochem 37, 891–911.

Wei, Z.B., Moldowan, J.M., Peters, K.E., Wang, Y., Xiang, W., 2007a. The abundance and distribution of diamondoids in biodegraded oils from the San Joaquin Valley: implications for biodegradation of diamondoids in petroleum reservoirs. Org. Geochem 38, 1910–1926.

Wei, Z.B., Moldowan, J.M., Zhang, S.C., Hill, R., Jarvie, D.M., Wang, H.T., Song, F.Q., Fago, F., 2007b. Diamondoid hydrocarbons as a molecular proxy for thermal maturity and oil cracking: geochemical models from hydrous pyrolysis. Org. Geochem 38, 227–249.

Williams, J.A., Bjorøy, M., Dolcater, D.L., Winters, J.C., 1986. Biodegradation in South Texas Eocene oils-effects on aromatics and biomarkers. Org. Geochem 10, 451–461.

Wingert, W.S., 1992. GC-MS analysis of diamondoid hydrocarbons in Smackover Petroleums. Fuel 71, 37–43.

Yang, W.L., Li, Y.K., Gao, R.Q., 1982. Formation and evolution of nonmarine petroleum in the Songliao Basin. China. J. Chang. Inst. Geol. 1, 69–79 (in Chinese with English abstract).

Zhang, S.C., Huang, H.P., Xiao, Z.Y., Liang, D.G., 2005. Geochemistry of Palaeozoic marin petroleum from the Tarim Basin, NW China. Part 2: maturity assessment. Org. Geochem 36, 1215–1225.